Title

Intermodality feature fusion combining unenhanced computed tomography and ferumoxytol-enhanced magnetic resonance angiography for patient-specific vascular mapping in renal impairment

Journal

Journal of Vascular Surgery, 71(5)

ISSN

0741-5214

Authors

Yoshida, Takegawa
Nguyen, Kim-Lien
Shahrouki, Puja
et al.

Publication Date

2020-05-01

DOI

10.1016/j.jvs.2019.08.240

Peer reviewed

HHS Public Access

Author manuscript

J Vasc Surg. Author manuscript; available in PMC 2022 October 20.

Published in final edited form as:

J Vasc Surg. 2020 May ; 71(5): 1674–1684. doi:10.1016/j.jvs.2019.08.240.

Inter-Modality Feature Fusion Combining Unenhanced CT and Ferumoxytol-Enhanced MRA for Patient-Specific Vascular Mapping in Renal Impairment

Takegawa Yoshida, MD[1,*], **Kim-Lien Nguyen, MD**[1,2,*], **Puja Shahrouki, MD**[1], **William J. Quinones-Baldrich, MD**[3], **Peter F. Lawrence, MD**[3], **J Paul Finn, MD**[1]

[1]Diagnostic Cardiovascular Imaging Laboratory, Department of Radiology, David Geffen School of Medicine at UCLA, Los Angeles, California, USA

[2]Division of Cardiology, David Geffen School of Medicine at UCLA and VA Greater Los Angeles Healthcare System, Los Angeles, California, USA

[3]Department of Vascular Surgery, David Geffen School of Medicine at UCLA

Abstract

Purpose: To establish the feasibility of fusing complementary, high-contrast features from unenhanced CT and ferumoxytol-enhanced magnetic resonance angiography (FE-MRA) for pre-procedural vascular mapping in patients with renal impairment.

Materials and methods: In this IRB-approved and HIPAA-compliant study, fifteen consecutive patients underwent both FE-MRA and unenhanced CT scanning, and the complementary high-contrast features from both modalities were fused to form an integrated, multi-feature image. Source images from CT and MR were segmented and registered. To validate the accuracy, precision and concordance of fused images to source images, unambiguous landmarks, such as wires from implantable medical devices (IMDs) or indwelling catheters, were marked on 3D models of the respective modalities, followed by rigid co-registration, interactive fusion, and fine adjustment. We then compared the positional offsets using pacing wires or catheters in the source FE-MRA (defined as points of interests, POIs) and fused images (n=5 patients, n=247 points). Points within 3D image space were referenced to the respective modalities: x (right-left), y (anterior-posterior), and z (cranial-caudal). The respective 3D orthogonal reference axes from

Corresponding author and reprint info: J. Paul Finn, MD, Department of Radiological Sciences, University of California at Los Angeles, Peter V. Ueberroth Building Suite 3371, 10945 Le Conte Ave., Los Angeles, CA 90095-7206, USA, Phone: 310.825.0958, Fax: 310.825.0880, pfinn@mednet.ucla.edu.

*Both authors contributed equally

AUTHOR CONTRIBUTIONS

Conception and design: JPF, KLN, TY

Analysis and interpretation: TY, KLN, JPF, WJQ, PFL

Data collection: TY, PS

Writing the article: KLN, TY

Critical revision of the article: all authors

Final approval of the article: all authors

Statistical analysis: TY, KLN

Obtained funding: not applicable

Overall responsibility: JPF, KLN

TY and KLN contributed equally to this article and share co-first authorship.

CONFLICTS OF INTEREST: The authors have no conflicts of interest to declare.

both image sets were aligned, such that with perfect registration a given point would have the same (x, y, z) component values in both sets. The 3-dimensional offsets (Δx mm, Δy mm, Δz mm) for each of the corresponding POIs represent non-concordance between the source FE-MRA and fused image. The offsets were compared using concordance correlation coefficients (CCC). Interobserver agreement was assessed using intraclass correlation coefficients (ICC) and Bland Altman analyses.

Results: Thirteen patients (age 76±12 years, 7 female) with aortic valve stenosis and chronic kidney disease (CKD) and 2 patients with thoracoabdominal vascular aneurysms and CKD underwent FE-MRA for pre-procedural vascular assessment and unenhanced CT exams were available in all patients. No ferumoxytol-related adverse events occurred. 247 matched POIs were evaluated on the source FE-MRA and fused images. In patients with IMDs, the mean offset in spatial position were: 0.31±0.51mm (ρ=0.99, C_b=1, 95% CI 0.99-0.99) for Δx, 0.27±0.69mm (ρ=0.99, C_b=0.99, 95% CI 0.99-0.99) for Δy, and 0.20±0.59mm (ρ=1, C_b=1, 95% CI 0.99–1.00) for Δz. Interobserver agreement was excellent (ICCs >0.99). The mean difference in offset between readers was 1.5mm.

Conclusions: Accurate 3D feature fusion is feasible, combining luminal information from FE-MRA with vessel wall information on unenhanced CT. This framework holds promise for combining the complementary strengths of MRI and CT to generate information-rich, multi-feature composite vascular images, while avoiding the respective risks and limitations of both modalities.

Table of Contents Summary

This cross-sectional retrospective study evaluated 15 patients with renal impairment and thoraco-abdominal vascular anomalies who underwent ferumoxytol-enhanced magnetic resonance angiography for pre-operative planning. All patients had unenhanced CT studies available. We demonstrate the feasibility of inter-modality feature fusion of vessel wall and lumen between unenhanced CT and ferumoxytol-enhanced magnetic resonance angiography for vascular mapping in patients with renal impairment.

Keywords

Inter-modality; image fusion; magnetic resonance angiography; computed tomography; ferumoxytol; vascular mapping; endovascular; transcatheter

INTRODUCTION

Whereas magnetic resonance angiography (MRA) provides excellent definition of the perfused vascular lumen, it is less sensitive to vascular calcification and may fail to image indwelling metal devices due to artifact.[1] The latter limitations can be significant for some important clinical applications.[2] For example, in candidates undergoing transcatheter aortic valve replacement (TAVR) and endovascular aneurysm repair (EVAR), multiple pre-procedural measurements are required to assess vascular morphology, determine the anatomic approach, and minimize the risk of complications. Both TAVR[3–5] and EVAR,[6, 7] require information such as patency, dimensions and tortuosity of arterial access vessels as well as the degree of vascular calcification. For EVAR, morphologic information such as

thrombus and complexity of the aneurysmal sac is crucial. Quantitative measurements are critical in determining EVAR device selection, deployment strategy, and surgical approach. 3D reconstruction after image acquisition facilitates accurate measurement of luminal dimensions in the presence of vessel tortuosity and the geometry of complex aneurysms can be appreciated from all points of view.[8] For complex EVAR procedures using fenestrated or branched endografts, advanced 3D reconstructions enable testing of endografts for adequate fitting and individualized graft design and have been shown to reduce Type 1 endoleaks.[9] To date, computed tomography (CT) has been preferentially used for EVAR planning even though many vascular patients have renal impairment and may require additional iodinated contrast in the operating theater.

Although contrast-enhanced MRA with gadolinium-based contrast agents (GBCAs) is widely implemented for vascular assessment, ferumoxytol-enhanced MRA has been proposed as a value-added alternative to GBCAs in patients with renal impairment.[10, 11] Ferumoxytol (Feraheme®; AMAG Pharmaceuticals, Inc., Cambridge, MA) is an ultrasmall super paramagnetic iron oxide (USPIO) approved by the US Food and Drug Administration (FDA) for treatment of iron deficiency anemia in patients with chronic kidney disease (CKD) and is a potent MR angiographic agent.[2, 12]

On the other hand, CT is exquisitely sensitive to calcium and can image a variety of indwelling hardware devices. However, CT angiography (CTA) requires injection of iodinated contrast agents, which are generally avoided in renal impairment due to the attendant risk of nephrotoxicity (exacerbating or precipitating renal failure). Similar concerns about the risk of nephrogenic systemic fibrosis (NSF) may limit the use of GBCA in this patient population. Although the incidence of nephrotoxicity following CTA can be up to 3.5%[13] and the incidence of NSF following GBCA ranges from 1–7% with linear gadolinium agents, the true incidence may be lower.[14] We hypothesize that in patients where ferumoxytol enhanced MRA (FE-MRA) is a suitable alternative to CTA,[12, 15] vascular calcification, bony anatomy and hardware devices may be accurately referenced to perfused luminal anatomy by fusing unenhanced CT and FE-MRA images. In a proof-of-concept study, we aim to evaluate the feasibility of combining luminal information from FE-MRA with vessel wall information on unenhanced CT to form an integrated, multi-feature image for pre-procedural planning in patients with disease of the aorta or aortic valve and renal impairment.

METHODS

Study population

This is a retrospective study, which was approved by our local Institutional Review Board and was compliant with the Health Insurance and Portability and Accountability Act (HIPPA). Consecutive patients who underwent both FE-MRA and unenhanced CT between January 2015 to August 2017 for vascular mapping were included (Table 1). All participants gave written informed consent. The patient population described in this manuscript has been partially included in two prior manuscripts. One focused on the safety profile of ferumoxytol as a diagnostic MR contrast agent;[16] the other assessed feasibility of FE-MRA (n=26) for TAVR planning in the setting of renal impairment.[17] Of the 26 patients from the prior TAVR

paper,[17] thirteen had available non-contrast CT studies performed previously and 5 of these had implanted cardiac devices. The subset of 13 patients, therefore, was used for validation of the registration algorithm described in the current work.

Image Acquisition

All patients had FE-MRI studies on a Siemens 3.0 Tesla scanner (Magnetom TIM Trio (n=3), Magnetom Prisma Fit (n=6) or Magnetom Skyra (n=1), Siemens Medical Solutions, Malvern, PA) or a 1.5 Tesla scanner (Magnetom TIM Avanto (n=5), Siemens Medical Solutions, Malvern, PA) for pre-operative vascular mapping. Patients had steady state MRA where ferumoxytol (4mg/kg) was given prior to MRI studies by slow intravenous infusion. Physiological monitoring of blood pressure, heart rate, pulse oximetry, and ECG was performed throughout all MRI procedures. FE-MRA involved 3D breath-held image acquisition with a product spoiled gradient echo sequence (repetition time 2.7ms, echo time 1.0ms, flip angle 19–20°, 1.0 × 1.3 × 1.2mm in-plane spatial resolution, bandwidth 610 Hz, 6/8 partial Fourier, GRAPPA acceleration factor 4). Two overlapping stations (150–200mm) with identical 3D spatial resolution (~1.0 × 1.2 × 1.3 mm) were acquired. Overlapping 3D FE-MRA data were combined into a single, 650 mm extended field of view (eFOV) image using commercial software (Image Compose, Siemens Medical Solutions, Inc).

Unenhanced CT studies were acquired on a Siemens Somatom Sensation 64 (n=7), Somatom Sensation 16 (n=1), Somatom Force (n=4), Aquilion (n=1) and Symbia T2 (n=1), with typical slice thickness ranging from 0.75 to 1.5 mm. CT imaging of the chest was carried out in 9 patients, and imaging of the abdomen and pelvis in 6 patients. In 12 patients, supero-inferior coverage on FE-MRA and CT was not the same and image fusion was therefore limited to the overlapping anatomy (n=3 had chest /abdomen /pelvis CT, n=4 had abdomen /pelvis CT, n=1 abdominal CT, n=7 pelvis CT).

FE-MRA and unenhanced CT volumetric data were available in the chest, abdomen, and pelvis (n=3); in the abdomen and pelvis (n=4); in the chest only (n=7); and in the abdomen only (n=1).

Image post-processing – Segmentation

Figure 1 outlines the framework for creating our feature fusion models. CT and FE-MRA source images were imported into commercially available software (Mimics v. 19.0; Materialise, Leuven, Belgium) for segmentation and rigid body image registration. To segment the regions of interest from the background structures, appropriate Hounsfield or grayscale signal intensity thresholds were assigned to CT or FE-MRA image datasets, such that voxels of similar intensity ranges were considered to be of the same structure (model-based region growing). The threshold values were set by two readers (TY, PS) for optimal visualization of calcifications and implanted medical devices (IMDs) on CT images, and for optimal reconstruction of enhanced blood vessels on FE-MRA images. Masks were defined and color-coded using the semi-automatic segment tool (C&V module, Mimics), and manually modified. Using the “Calculate 3D” (Mimics, Materialise) function, 3D triangle-based models from each CT and FE-MRA dataset were reconstructed based on pre-defined masks (Figure 1, Online video S1).

Image post-processing – Co-registration of segmented FE-MRA and CT datasets

To co-register the segmented CT and MRA datasets, we manually specified anatomic landmarks[18] on both the segmented CT and FE-MRA 3D models using points within Mimics. Specific landmarks varied by cases. For example, in patients with visible calcifications involving the ascending aorta extending to the brachiocephalic artery, left common carotid artery or left subclavian artery, we marked the respective ostia of these branches as fiducial landmarks. Where present, we also used calcifications on the aortic valve and the ostia of the coronary arteries, celiac artery, renal arteries, and iliac arteries as landmarks. We then used the semi-automatic registration tools in Mimics to initiate the co-registration, followed by manual fine adjustments after visual inspection (Figure 1, Online video S1). The resulting co-registered datasets had corresponding spatial resolution, orientation, and dimension; each point within the co-registered 3D imaging volume can be described using x, y, z coordinates.[19] We exported the co-registered datasets from Mimics as DICOMs and imported them into OsiriX (OsiriX, Geneva, Switzerland) for further validation.

Validation using intrinsic rigid landmarks

To validate the accuracy, precision and concordance of fused images, we compared the positions of pacing wires or catheters in the original FE-MRA (defined as points of interests, POIs) and fused images (n=5 patients, n=247 points). These cases were chosen because they produced defined and unambiguous signal changes on the respective modalities. On FE-MRA images, IMDs produce a signal void (Figure 2, green arrows), whereas on CT and consequently in the fused images, the dense IMDs produce high intensity pixels (Figure 2, red arrows). One reader (TY) defined the POI within 3D image space using Cartesian coordinates referenced to the respective modalities: x (right-left), y (anterior-posterior), and z (cranial-caudal). The respective 3D orthogonal reference axes from both image sets were aligned and had the same zero point, such that with perfect registration a given point would have the same (x, y, z) component values in both sets. The 3-dimensional offsets (Δx mm, Δy mm, Δz mm) for each of the corresponding points of interest were used to quantify non-concordance between the original FE-MRA and fused image. To evaluate for inter-observer agreement of the offsets, a second reader (PS) independently determined POIs (n=50) on FE-MRA and fused images of one patient; the offsets were compared.

Statistical analysis

MedCalc Statistical Software version 17.2 (MedCalc©, Ostend, Belgium) was used for the statistical analyses. The offsets between two paired POIs in the x, y and z dimension, and in 3D space, were evaluated for normality using the Shapiro-Wilk test. To compare intra-subject offsets, analysis of variance (ANOVA) and the Friedman test were used for parametric and nonparametric data where appropriate. For inter-subject analyses, the concordance correlation coefficient (CCC) was calculated. The CCC contains the Pearson's rho (ρ) correlation coefficient and bias correction factor (C_b), which are measures of precision and accuracy respectively. Inter-observer agreement was assessed using intraclass correlation coefficients (ICCs) in a two-way mixed-method model with absolute agreement

and bias was assessed using Bland-Altman plots. Data are reported either as mean ± standard deviation (SD) or median and interquartile range (IQR).

RESULTS

A total of 15 patients (age 74±12 years, 8 female) with either aortic valve stenosis or aortic aneurysm and CKD underwent FE-MRA and unenhanced CT for pre-procedural vascular assessment from January 2015 until August 2017 (Table 1). The median time span between the FE-MRA and unenhanced CT was 4 days (IQR 0–28 days). All patients underwent FE-MRA without any adverse events. Of the 15 CKD patients, 3 were hemodialysis-dependent, 3 had renal transplants, and the remaining patients had estimated glomerular filtration rates (eGFRs) ranging from 20 to 78 mL/min/1.73m^2. None of the patients had a history of allergy to iron agents. A subset of five patients who had IMDs (n=4) or femoral catheter (n=1) was used for assessment of image fusion accuracy.

Image fusion

In all cases, 3D models of the arteries, veins and cardiac chambers were separately created from FE-MRA for visualization of perfused luminal anatomy from an arbitrary angle. On corresponding unenhanced CT images, vascular and valvular calcifications together with the pacing wires or catheters were segmented and similarly converted to 3D models. Subsequently, the entire vasculature was successfully fused with the calcifications and pacing wires or catheters, without the need for changes in scale or form. Figures 3–6 and Online video S1–S3 show illustrative examples of fused 3D models that demonstrate the quality of fusion images with strong visual confirmation of the locations of vascular calcification, aneurysmal dilation and IMDs, as well as visualization of vessel tortuosity. The segmentation time for the 15 cases ranged between 2 to 3 hours.

Offsets between intrinsic rigid landmarks and fused image models

A total of 247 matched POIs were evaluated on the original FE-MRA and fused images (Figure 7). Both inter-subject and intra-subject offsets were small. The mean inter-subject 3-dimensional POI-based offset was 0.64 ± 0.92 mm (ranging from 0.05 to 5.49 mm). Offsets for each dimension were $\Delta x = 0.31 \pm 0.51$ mm (ranging from 0.00 to 4.02 mm), $\Delta y = 0.27 \pm 0.69$ mm (ranging from 0.00 to 4.17 mm), and $\Delta z = 0.20 \pm 0.59$ mm (ranging from 0.00 to 3.98 mm) for X, Y and Z dimensions respectively. The mean Z-dimension offset (1.85 mm) was significantly lower ($p<0.05$) than both X (2.08 mm) and Y (2.07 mm). Concordance of offsets between subjects in each dimension was excellent: X, $\rho=0.9997$ ($C_b=1$, 95% CI 0.9996–0.9998); Y, $\rho=0.9994$ ($C_b=0.9999$, 95% CI 0.9992–0.9995); and Z, $\rho=1$ ($C_b=1$, 95% CI 0.9999–1.0000). Differences for within-subject 3D offsets were statistically significant ($P<0.01$, Figure 8), but not clinically relevant (range of mean intra-subject offsets 0.38 to 1.23 mm). Interobserver agreement for the POIs was excellent for all dimensions on FE-MRA (X, ICC 0.9994 [95% CI 0.9989–0.9997]; Y, ICC 0.9942 [95% CI 0.9897–0.9968]; Z ICC 0.9998 [95% CI 0.9997–0.9999]) and in fused models (X, ICC 0.9999 [95% CI 0.9999–1.0000]; Y, ICC 0.9998 (95% CI 0.9996–0.9999); Z, ICC 1 [95% CI 1.0000–1.0000]). The mean difference in registration offset between readers was -1.5mm

(lower limit of agreement -3.84mm [95% CI -1.83 to -1.11mm]; upper limit of agreement 0.91 mm [95% CI 0.29 to 1.5mm]) with a repeatability coefficient of 3.7.

DISCUSSION

The results of our study suggest that fusion of luminal information from FE-MRA and vessel wall information from unenhanced CT can generate highly accurate and reproducible image integration of all relevant structures for pre-procedural vascular planning. The use of FE-MRA with unenhanced CT is especially attractive in patients with renal impairment where there are concerns about iodinated contrast media and GBCAs and where vascular calcification may be florid and widespread. As the purpose of our study was to report the feasibility of feature-based fusion imaging, the patient sample size is relatively modest. Further, because the method for validation of the fusion offsets between vasculature and calcifications has not been previously established, our work was limited to evaluations of the offsets of pacemakers and catheters between original and fused images.

Inter-subject and intra-subject offsets varied, but the mean offsets in all three dimensions (x, y, and z) and 3D offsets were not clinically relevant. These variations were related to known challenges for inter-modality 3D-3D image registration. The method of placing the ROIs may have been contributory. As the pacing coil and femoral catheter primarily extend vertically, corresponding to the Z-dimension, the ROIs were consecutively marked in axial planes for fixed slice intervals. This may explain why the offsets in the z-dimension were significantly smaller than in the other dimensions. The inter-subject offsets could be explained by the different shapes of the IMDs and the fact that neither the FE-MRA or unenhanced CT acquisitions were cardiac gated and the gantry angle for CT images was not corrected during co-registration. For the intracardiac portion of the pacing wires, therefore, one would anticipate a real difference between the x-y configuration of the wires, depending on where in the cardiac cycle the acquisition was centered. This error would be expected both between the modalities and within the modalities, at different time points. The use of pacing wires, therefore, does not reflect a best-case choice for a reference variable, but the fact that errors were small even within this constraint is reassuring. One would expect that this source of error would be minimal or disappear for structures that vary little over the cardiac or respiratory cycles (for example the aorto-iliac system). Conversely, one would expect structures that vary substantially over the respiratory or cardiac cycle (e.g. liver or cardiac chambers) would be more susceptible to inconsistent cardiac or respiratory phase as a source of offset error.

It should be noted that the differences between the mean offsets were in the range of 0.48 to 0.99mm, which in the current context was not clinically significant, is consistent with prior work reporting a registration error up to 1.43mm using the root mean square method.[20] Pragmatically, the limits of acceptable registration error should be defined on case by case basis, depending on the clinical questions. For example, fusing MR and CT images of the coronary arteries would invoke more stringent requirements in terms of spatial and temporal resolution than is the case for the abdominal aorta or femoral arteries. Nonetheless, the same principles would apply, assuming acceptable image quality can be achieved.

Although the registration in our study took typically less than 5 minutes, the image segmentation was far more time consuming and will require workflow optimization strategies for time sensitive clinical applications. However, with steady advances in image segmentation algorithms and processing power, and with the imminent implementation of deep learning strategies, it seems likely that the engineering bottlenecks will be short lived.

Over the past decade, the benefits and limitations of CMR and CTA have been extensively debated. Iodine or gadolinium-based contrast agents are often required for CTA and MRA respectively, which may be problematic in patients with renal impairment because of the risk of post-procedural renal failure or NSF.[21] This is especially relevant in TAVR candidates, as renal impairment is frequent in patients with aortic stenosis.[22, 23] Ferumoxytol has unique properties as a contrast agent for MRA as compared to GBCA, and may be a suitable alternative to CTA in patients with renal impairment.[10, 16] Recently, FE-MRA has been proposed as a suitable, renal safe diagnostic tool for pre-TAVR assessment, where vascular access planning can be successfully completed.[17, 24]

There have been earlier reports of image fusion between FE-MRA and fluoroscopy,[25] CT and fluoroscopy,[26] ultrasound and fluoroscopy,[27] as well as contrast-enhanced coronary CTA with perfusion gadolinium-enhanced MR.[28] Our study however, is unique in proposing a 3D-3D feature-based strategy for generating a complete, integrated, multi-parameter vascular model from FE-MRA and unenhanced CT. This allows for augmented a priori, pre-procedural planning with evaluation of all relevant vessels, together with vascular calcifications, bony anatomy and IMDs as shown in Online video S1. The value of our framework for vascular models lies not only in the advanced visualization, but also in the non-nephrotoxic way in which the images could be acquired and with minimal radiation from unenhanced CT exams that may already have been performed for other clinical reasons.

An intriguing aspect of fusing CT with MR images is that the integrated images contain more information than either modality alone, while maintaining high spatial resolution in a readily compatible, natural-appearing display. While MR and CT images are both potentially high resolution and volumetric, they each have well known strengths and weaknesses, which tend to be complementary, in that they have their high-contrast sweet spots in different parts of the tissue spectrum. The potential clearly exists to build upon the single modality thumbprints of, for example, plaque and thrombus, by incorporating the features visible on either the MR or CT moieties of the complex image. For now, these questions remain in the research realm, but the clinical implications are compelling. For our study, integration of the detailed luminal anatomy seen on FE-MRA with the vascular calcifications and IMDs seen on unenhanced CT enabled a more confident and complete assessment of structural disease was possible than with either modality alone. The intuitive and graphic display is appealing to surgeons and interventionists and may inform previously unanticipated challenges or revised approaches to procedural pathways. The clinical impact of these feature-rich datasets will require validation in more extensive studies.

Our study has limitations. As the purpose of our study was to report the feasibility of fusion images, the sample size is relatively modest. Further, because the method for validation of

the fusion offsets between vasculature and calcifications has not been previously established, our work was limited to evaluations of the offsets of pacemakers and catheters between original and fused images. However, the measured accuracy of our technique was very high and was further validated by an equally high inter-observer agreement. The spatial resolution for our FE-MRA was sufficiently high (1.0 x 1.2 x 1.3mm) that abnormalities in mesenteric or renal arteries can be readily appreciated. In our current study group, the FE-MRA and CT datasets were not cardiac gated because, at the time a breath-held 3D gated MRA sequence was not available to us and the unenhanced CT exams were performed for other indications where gating was not necessary. Since completion of our study, we have implemented a breath-held, gated 3D MRA technique which we now use routinely when evaluating the thoracic aorta with ferumoxytol. Acquisition of images using 4D MRI[29, 30] may also address the issue of cardiac gating, but was not performed in our current set of patients.

In suitable patients of a younger age group where minimization of radiation exposure assumes even greater importance, fusion of FE-MRA with low dose unenhanced CT may be an attractive option, as only landmarks of high attenuation are needed for successful fusion. With minimal radiation and renal safety, the scope for inter-modality 3D feature fusion could expand to encompass broad and as yet undefined clinical applications.

CONCLUSION

In conclusion, our study demonstrates high accuracy for complementary feature fusion of vessel lumen from FE-MRA and vessel wall from unenhanced CT. These 3D fused models and the framework for feature-based fusion have immediate implications for precise anatomic localization of vascular calcification, aortic aneurysm and implantable medical devices.

Supplementary Material

Refer to Web version on PubMed Central for supplementary material.

FUNDING:

This is an unfunded study. Data were derived in the context of clinical care. Dr. Kim-Lien Nguyen and Dr. J. Paul Finn are supported by a grant from the American Heart Association (AHA 18TPA34170049).

REFERENCES

1. Rogers T, Waksman R. Role of CMR in TAVR. JACC Cardiovascular imaging. 2016;9(5):593–602. [PubMed: 27151522]
2. Bashir MR, Bhatti L, Marin D, Nelson RC. Emerging applications for ferumoxytol as a contrast agent in MRI. J Magn Reson Imaging. 2015 Apr;41(4):884–98. [PubMed: 24974785]
3. Holmes DR Jr., Mack MJ, Kaul S, Agnihotri A, Alexander KP, Bailey SR, et al. 2012 ACCF/AATS/SCAI/STS expert consensus document on transcatheter aortic valve replacement. J Am Coll Cardiol. 2012;59(13):1200–54. [PubMed: 22300974]
4. Kasel AM, Cassese S, Bleiziffer S, Amaki M, Hahn RT, Kastrati A, et al. Standardized imaging for aortic annular sizing: implications for transcatheter valve selection. JACC Cardiovasc Imaging. 2013;6(2):249–62. [PubMed: 23489539]

5. Piazza N, de Jaegere P, Schultz C, Becker AE, Serruys PW, Anderson RH. Anatomy of the aortic valvar complex and its implications for transcatheter implantation of the aortic valve. Circ Cardiovasc Interv. 2008;1(1):74–81. [PubMed: 20031657]
6. Francois CJ, Skulborstad EP, Majdalany BS, Chandra A, Collins JD, Farsad K, et al. ACR Appropriateness Criteria((R)) Abdominal Aortic Aneurysm: Interventional Planning and Follow-Up. J Am Coll Radiol. 2018;15(5s):S2–s12. [PubMed: 29724423]
7. Chaikof EL, Dalman RL, Eskandari MK, Jackson BM, Lee WA, Mansour MA, et al. The Society for Vascular Surgery practice guidelines on the care of patients with an abdominal aortic aneurysm. J Vasc Surg. 2018;67(1):2–77.e2. [PubMed: 29268916]
8. Sobocinski J, Chenorhokian H, Maurel B, Midulla M, Hertault A, Le Roux M, et al. The benefits of EVAR planning using a 3D workstation. Eur J Vasc Endovasc Surg. 2013;46(4):418–23. [PubMed: 23972762]
9. Greenberg RK, Sternbergh WC 3rd, Makaroun M, Ohki T, Chuter T, Bharadwaj P, et al. Intermediate results of a United States multicenter trial of fenestrated endograft repair for juxtarenal abdominal aortic aneurysms. J Vasc Surg. 2009;50(4):730–7.e1. [PubMed: 19786236]
10. Finn JP, Nguyen KL, Han F, Zhou Z, Salusky I, Ayad I, et al. Cardiovascular MRI with ferumoxytol. Clin Radiol. 2016;71(8):796–806. [PubMed: 27221526]
11. Finn JP, Nguyen KL, Hu P. Ferumoxytol vs. Gadolinium agents for contrast-enhanced MRI: Thoughts on evolving indications, risks, and benefits. J Magn Reson Imaging. 2017;46(3):919–23. [PubMed: 28160356]
12. Toth GB, Varallyay CG, Horvath A, Bashir MR, Choyke PL, Daldrup-Link HE, et al. Current and potential imaging applications of ferumoxytol for magnetic resonance imaging. Kidney Int. 2017;92(1):47–66. [PubMed: 28434822]
13. McDonald JS, McDonald RJ, Carter RE, Katzberg RW, Kallmes DF, Williamson EE. Risk of intravenous contrast material-mediated acute kidney injury: a propensity score-matched study stratified by baseline-estimated glomerular filtration rate. Radiology. 2014;271(1):65–73. [PubMed: 24475854]
14. American College of Radiology. ACR Manual on Contrast Media (Version 10.3). 2017. Accessed January 27, 2018.Available from: https://www.acr.org/media/ACR/Files/Clinical-Resources/Contrast_Media.pdf.
15. Nguyen KL, Moriarty JM, Plotnik AN, Aksoy O, Yoshida T, Shemin RJ, et al. Ferumoxytol-enhanced MR Angiography for Vascular Access Mapping before Transcatheter Aortic Valve Replacement in Patients with Renal Impairment: A Step Toward Patient-specific Care. Radiology. 2018 Jan;281(1):326–337.
16. Nguyen KL, Yoshida T, Han F, Ayad I, Reemtsen BL, Salusky IB, et al. MRI with ferumoxytol: A single center experience of safety across the age spectrum. J Magn Reson Imaging. 2017;45(3):804–12. [PubMed: 27480885]
17. Nguyen KL, Moriarty JM, Plotnik AN, Aksoy O, Yoshida T, Shemin RJ, et al. Ferumoxytol-enhanced MR Angiography for Vascular Access Mapping before Transcatheter Aortic Valve Replacement in Patients with Renal Impairment: A Step Toward Patient-specific Care. Radiology. 2018;286(1):326–37. [PubMed: 29040038]
18. Hill DL, Hawkes DJ, Crossman JE, Gleeson MJ, Cox TC, Bracey EE, et al. Registration of MR and CT images for skull base surgery using point-like anatomical features. The British Journal of Radiology. 1991;64(767):1030–5. [PubMed: 1742584]
19. Arun KS HTS, Blostein S.D. Least-squares fitting of two 3D point sets. IEEE Transactions of Pattern Analysis and Machine Intelligence. 1987(PAMI-9):698–700.
20. Ruijters D, Homan R, Mielekamp P, van de Haar P, Babic D. Validation of 3D multimodality roadmapping in interventional neuroradiology. Phys Med Biol. 2011;56(16):5335–54. [PubMed: 21799235]
21. Sinning JM, Ghanem A, Steinhauser H, Adenauer V, Hammerstingl C, Nickenig G, et al. Renal function as predictor of mortality in patients after percutaneous transcatheter aortic valve implantation. JACC Cardiovascular Interventions. 2010;3(11):1141–9. [PubMed: 21087750]

22. Nguyen TC, Babaliaros VC, Razavi SA, Kilgo PD, Guyton RA, Devireddy CM, et al. Impact of varying degrees of renal dysfunction on transcatheter and surgical aortic valve replacement. The Journal of thoracic and cardiovascular surgery. 2013;146(6):1399–406. [PubMed: 24075566]

23. Thourani VH, Keeling WB, Sarin EL, Guyton RA, Kilgo PD, Dara AB, et al. Impact of preoperative renal dysfunction on long-term survival for patients undergoing aortic valve replacement. Ann Thorac Surg. 2011;91(6):1798–806. [PubMed: 21536247]

24. Kallianos K, Henry TS, Yeghiazarians Y, Zimmet J, Shunk KA, Tseng EE, et al. Ferumoxytol MRA for transcatheter aortic valve replacement planning with renal insufficiency. International journal of cardiology. 2017;231:255–7. [PubMed: 28100426]

25. Schwein A, Chinnadurai P, Shah DJ, Lumsden AB, Bechara CF, Bismuth J. Feasibility of three-dimensional magnetic resonance angiography-fluoroscopy image fusion technique in guiding complex endovascular aortic procedures in patients with renal insufficiency. J Vasc Surg. 2017;65(5):1440–52. [PubMed: 28017584]

26. Glockler M, Halbfabeta J, Koch A, Achenbach S, Dittrich S. Multimodality 3D-roadmap for cardiovascular interventions in congenital heart disease--a single-center, retrospective analysis of 78 cases. Catheterization and Cardiovascular Interventions. 2013;82(3):436–42. [PubMed: 22936634]

27. Jone PN, Ross MM, Bracken JA, Mulvahill MJ, Di Maria MV, Fagan TE. Feasibility and Safety of Using a Fused Echocardiography/Fluoroscopy Imaging System in Patients with Congenital Heart Disease. Journal of the American Society of Echocardiography. 2016;29(6):513–21. [PubMed: 27143284]

28. von Spiczak J, Manka R, Gotschy A, Oebel S, Kozerke S, Hamada S, et al. Fusion of CT coronary angiography and whole-heart dynamic 3D cardiac MR perfusion: building a framework for comprehensive cardiac imaging. International Journal of Cardiovascular Imaging. 2018;34(4):649–60. [PubMed: 29080955]

29. Han F, Zhou Z, Han E, Gao Y, Nguyen KL, Finn JP, et al. Self-gated 4D multiphase, steady-state imaging with contrast enhancement (MUSIC) using rotating cartesian K-space (ROCK): Validation in children with congenital heart disease. Magnetic Resonance in Medicine. 2017;78(2):472–83. [PubMed: 27529745]

30. Zhou Z, Han F, Rapacchi S, Nguyen KL, Brunengraber DZ, Kim GJ, et al. Accelerated ferumoxytol-enhanced 4D multiphase, steady-state imaging with contrast enhancement (MUSIC) cardiovascular MRI: validation in pediatric congenital heart disease. NMR in biomedicine. 2017;30(1).

ARTICLE HIGHLIGHTS

Type of Research:

Cross-sectional retrospective study

Key Findings:

Inter-modality fusion of complimentary features from unenhanced CT and ferumoxytol-enhanced magnetic resonance angiography is feasible and offers a best-of-both-modalities, non-nephrotoxic approach for augmented peri-operative vascular mapping in patients with vascular disease and impaired renal function.

Take Home Message:

Inter-modality feature fusion from unenhanced CT and ferumoxytol-enhanced magnetic resonance angiography can be used to provide safe and comprehensive vessel wall and lumen imaging in patients with thoraco-abdominal vascular diseases and renal impairment.

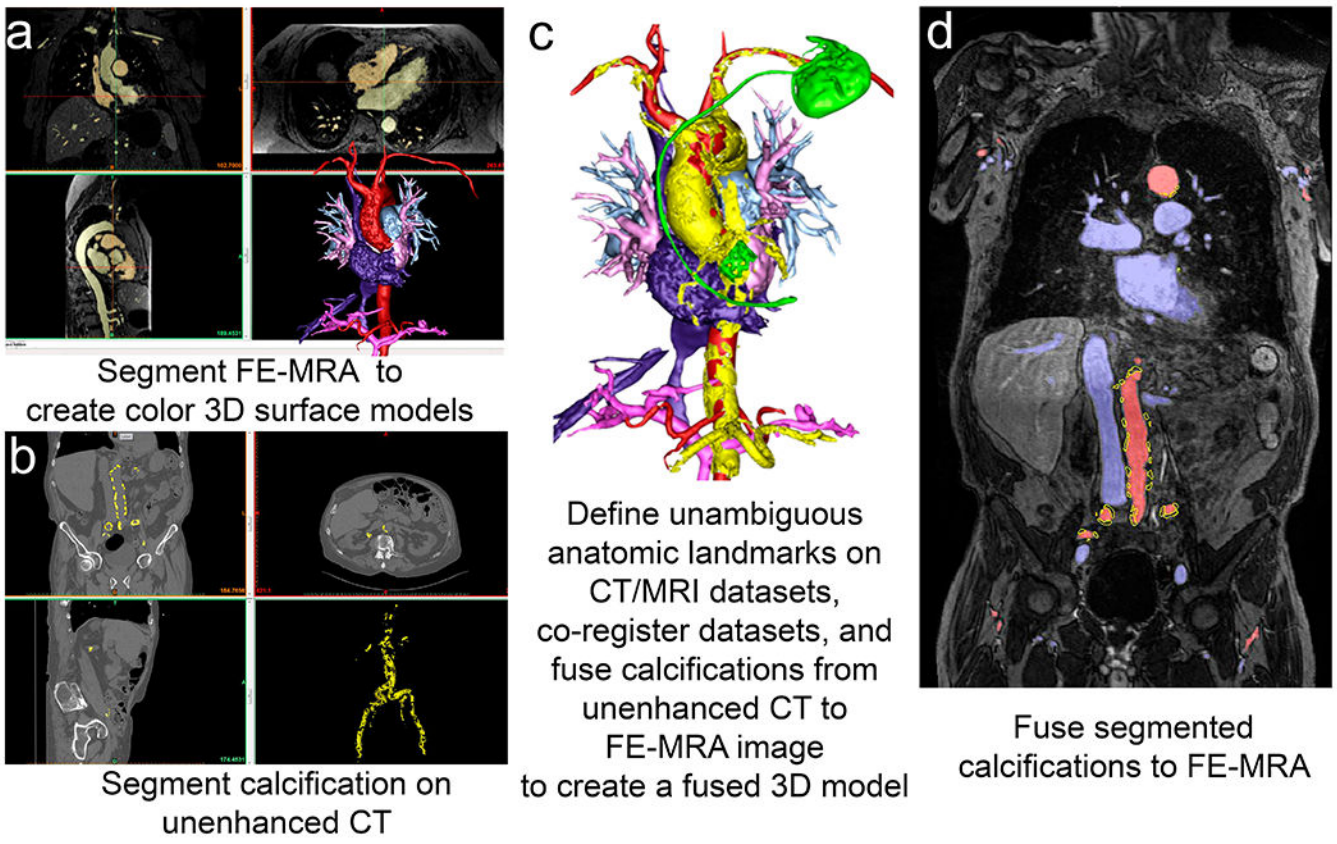

Fig 1.

Steps for inter-modality feature fusion with unenhanced CT and ferumoxytol-enhanced MRA (a-d). Online video S1 shows selective feature fusion of the arterial bed (a), venous system (b), and bony structures into an integrative 3D surface model (d).

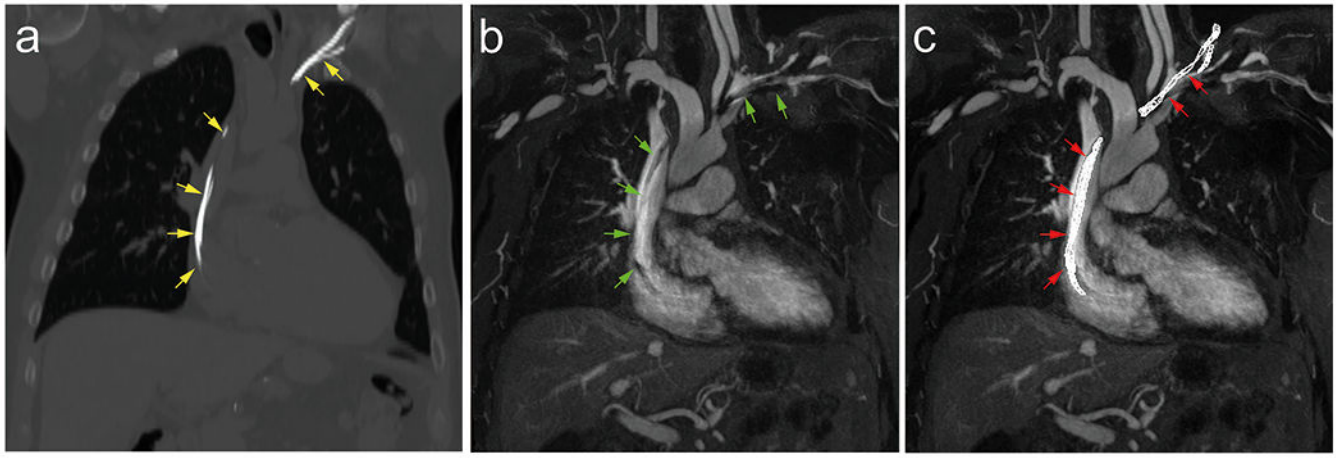

Fig 2.

60-year-old male patient with renal impairment, critical aortic valve stenosis and a pacing wire in the left innominate vein, superior vena cava and right heart. Rigid registration is based on selected features from unenhanced CT (a) and original FE-MRA (b) images. The pacing coil seen in the unenhanced CT (a, yellow arrows) was accurately fused with the signal void in the FE-MRA (b, green arrows) to form the fused image (c, red arrows).

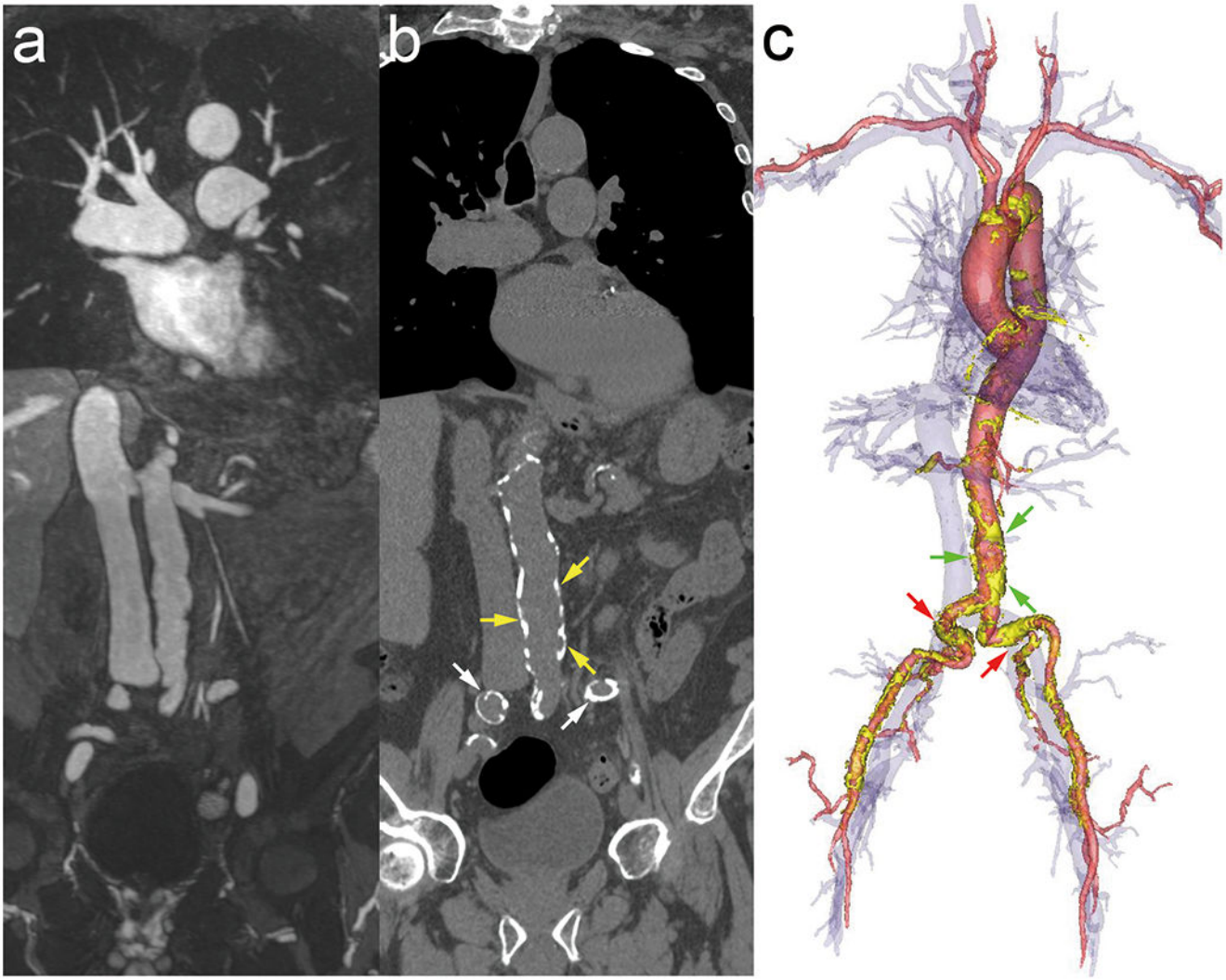

Fig 3.

FE-MRA (a), unenhanced CT (b) and a fused 3D model (c) belonging to an 80-year-old male with severe aortic valve stenosis and moderate renal impairment. The fused 3D model from FE-MRA and unenhanced CT shows the entire aorta and pelvic access vessels with atherosclerotic calcification, most severe in the iliac arteries. The calcification of the abdominal aorta (yellow arrows) and both iliac arteries (white arrows) from the CT image can be clearly defined on the fused 3D model (green and red arrows respectively).

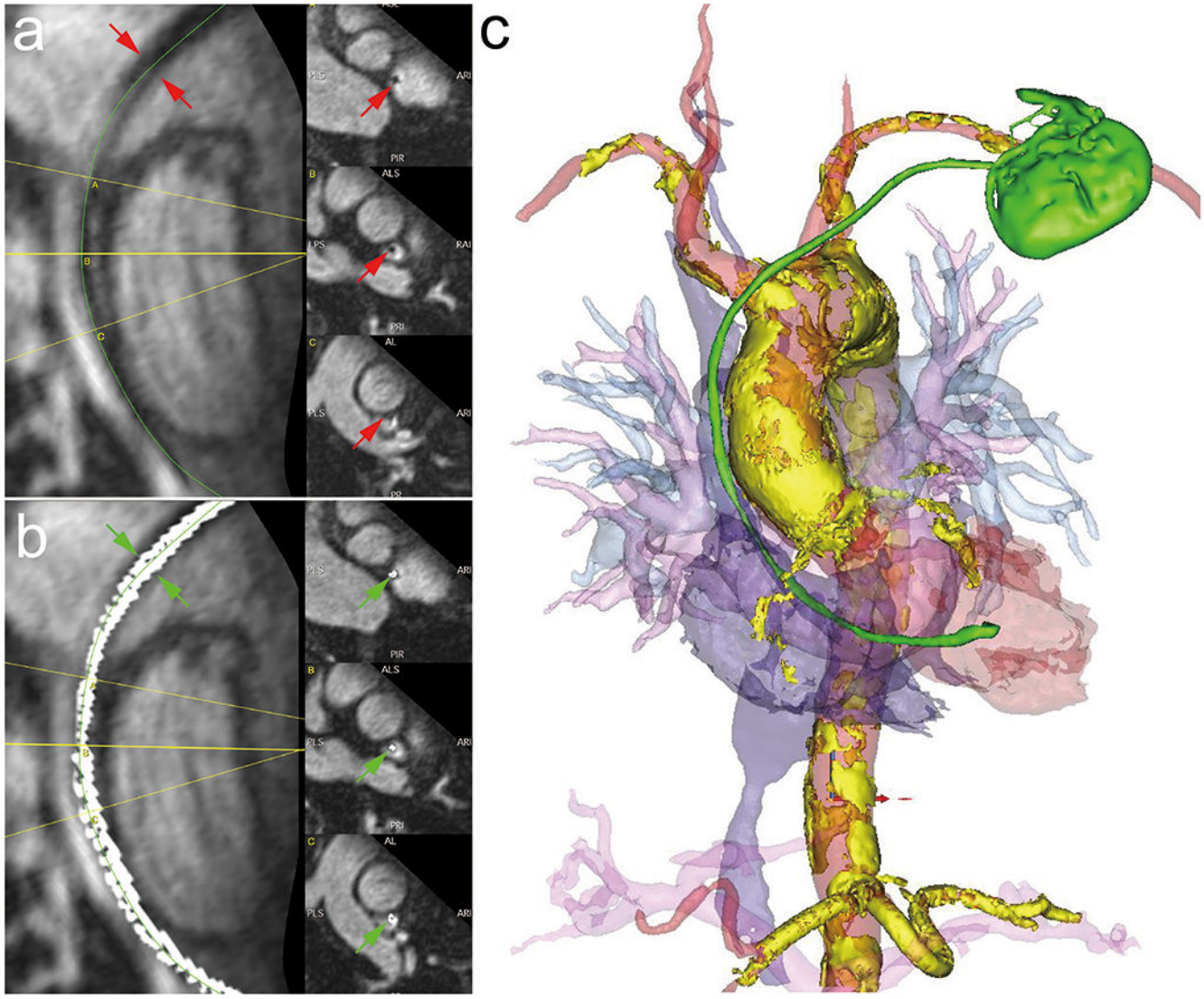

Fig 4.

A 3D curved multi-planar reconstruction (MPR) of original FE-MRA (a) and fused image (b), and a fused 3D model (c) belonging to a 78-year-old female with symptomatic aortic valve stenosis, moderate renal impairment and a pacemaker, status post TAVR. The signal void (red arrows) and an accurately fused pacing coil (green arrows) are defined on the FE-MRA and fused image respectively. The fused 3D model demonstrates a heavily calcified aorta, and the relationship between calcification, vasculature, pacemaker and the prosthetic aortic valve can be clearly visualized. Online video S2 shows a 360° view of the fused 3D model.

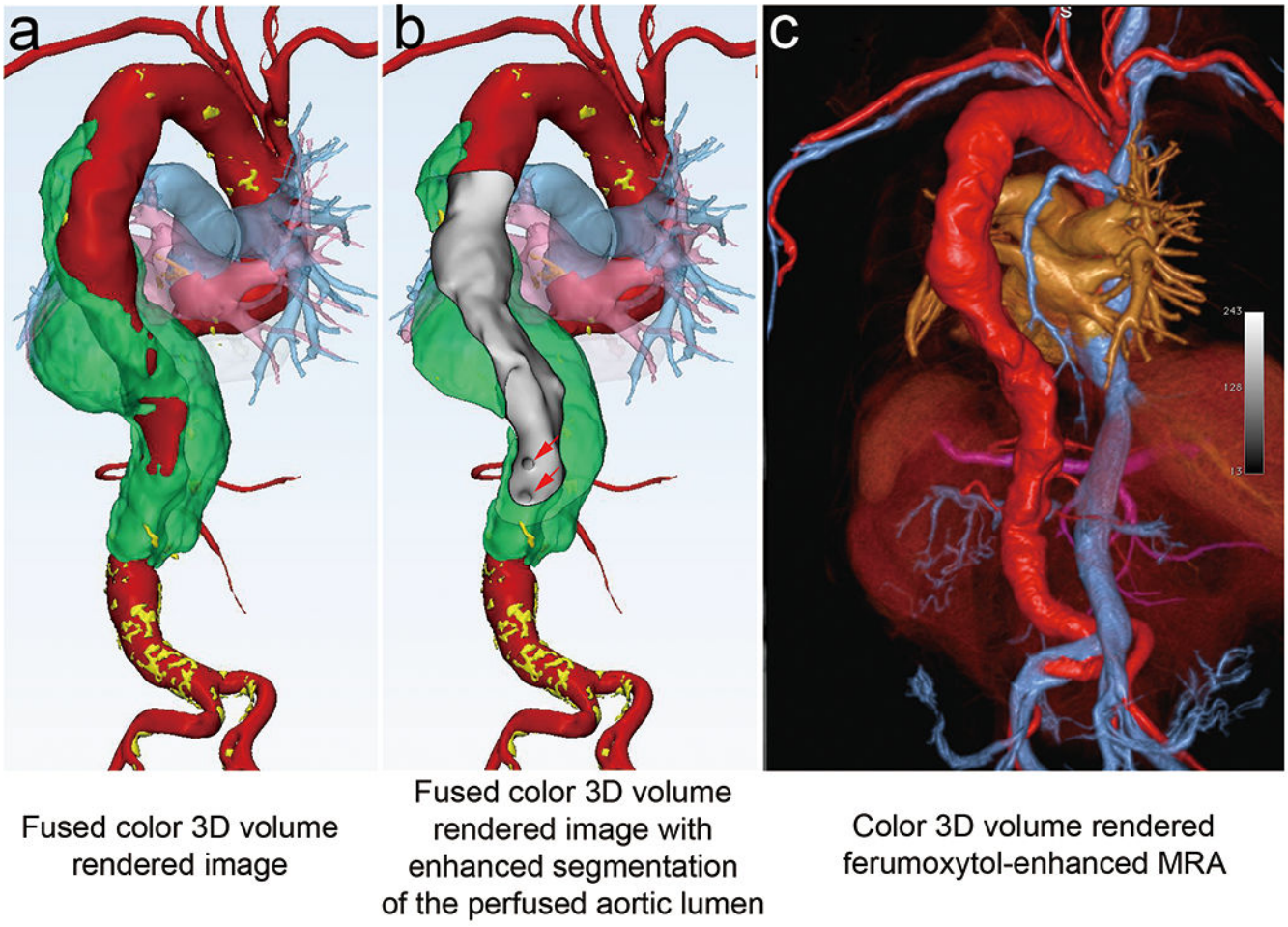

Fig 5.

A fused 3D model belonging to an 83-year-old male shows a large, predominantly fusiform thoracoabdominal aortic aneurysm and renal impairment. The fused 3D model (posterior view) shows the entire extent of the aortic aneurysm with atherosclerotic calcifications (a-b, yellow regions). The aortic aneurysm and calcifications are shown extending from the top of the thoracic aorta to the middle of the abdominal aorta. The relationship between each anatomical structure can be more clearly defined by showing the perfused aortic lumen (b, gray color) and the origin of the celiac trunk and superior mesenteric artery (b, red arrows). Extensive thrombus within the aneurysm is rendered in green and was derived from the MRA data. Ferumoxytol-enhanced MRA image (c) shows both arterial and venous perfused anatomy (excluding the mural thrombus). Through color 3D volume rendering with segmentation of extracted features from each modality (a-b), the desired spatial relationships are enhanced. Online video S3 shows a 360° view of the fused 3D image (a-b).

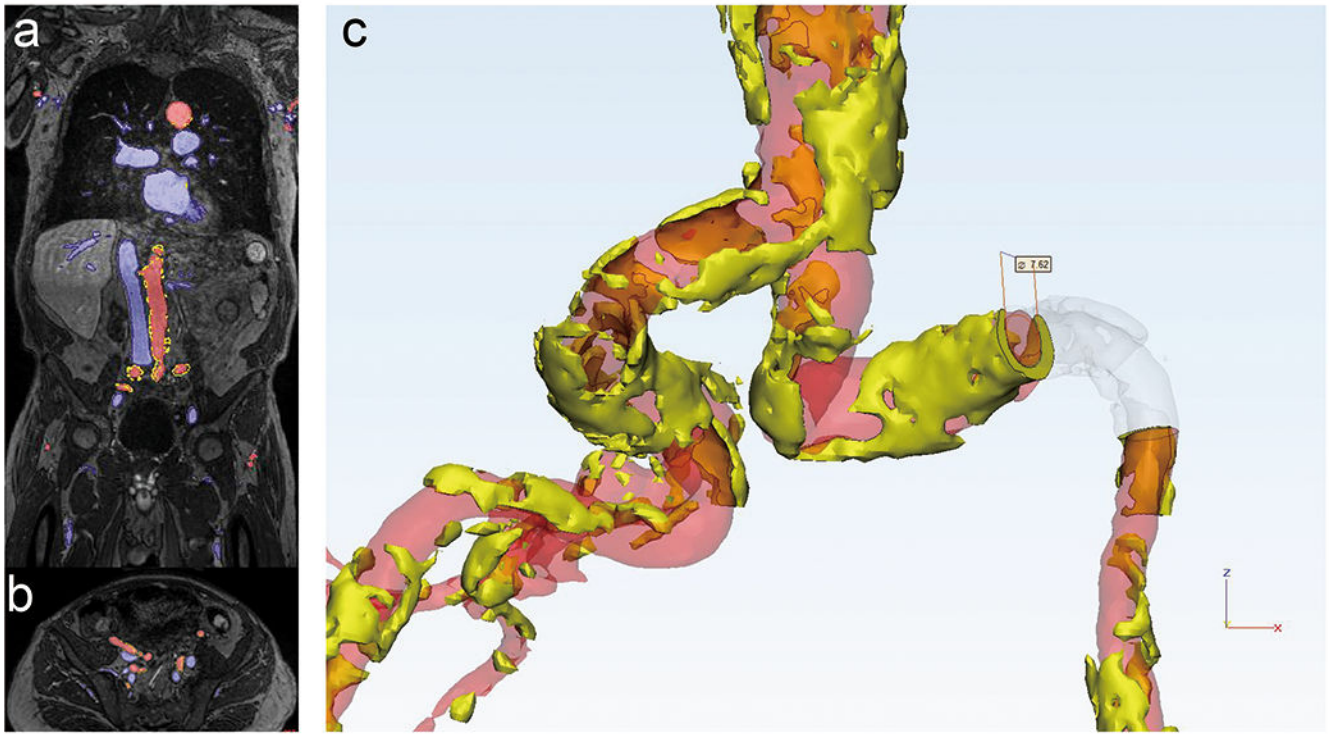

Fig 6.

Segmentation of vasculature in FE-MRA from coronal view (a) and axial view (b), and fused 3D model (c). These images belong to an 80-year-old male with severe aortic valve stenosis and moderate renal impairment. A detailed fused 3D model of the entire aortoiliofemoral vasculature overlaid with calcification is displayed. Vessel tortuosity, calcific burden and morphology, as well as the presence of complex calcific atheroma could be clearly defined and measured.

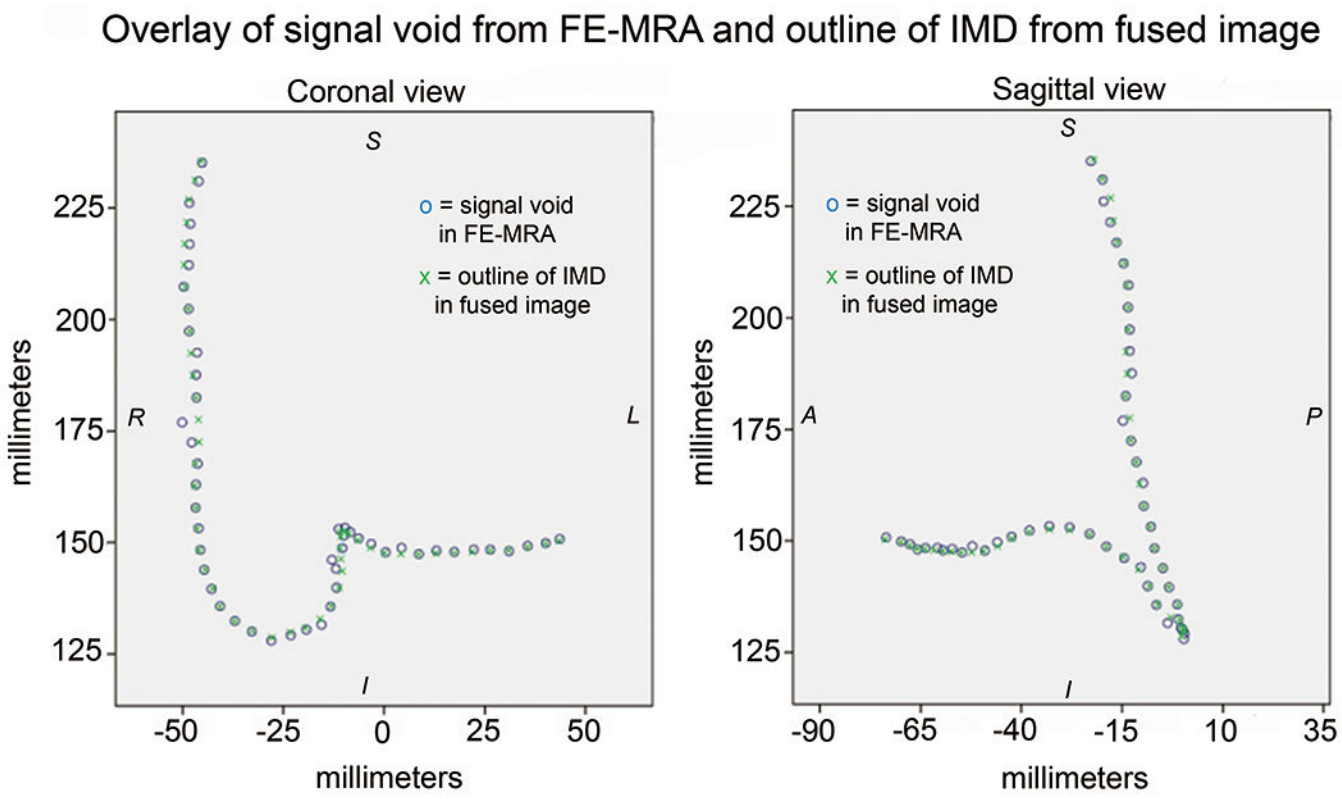

Fig 7.

Overlay of points of interests (POIs) on original FE-MRA relative to fused image models from one subject. The POIs from the original FE-MRA (blue circles) and fused image (green x) from coronal and sagittal views show overlap with minimal offsets. *A*, anterior; *I*, inferior; *IMD*, implanted medical devices; *L*, left; *P*, posterior; *R*, right; *S*, superior

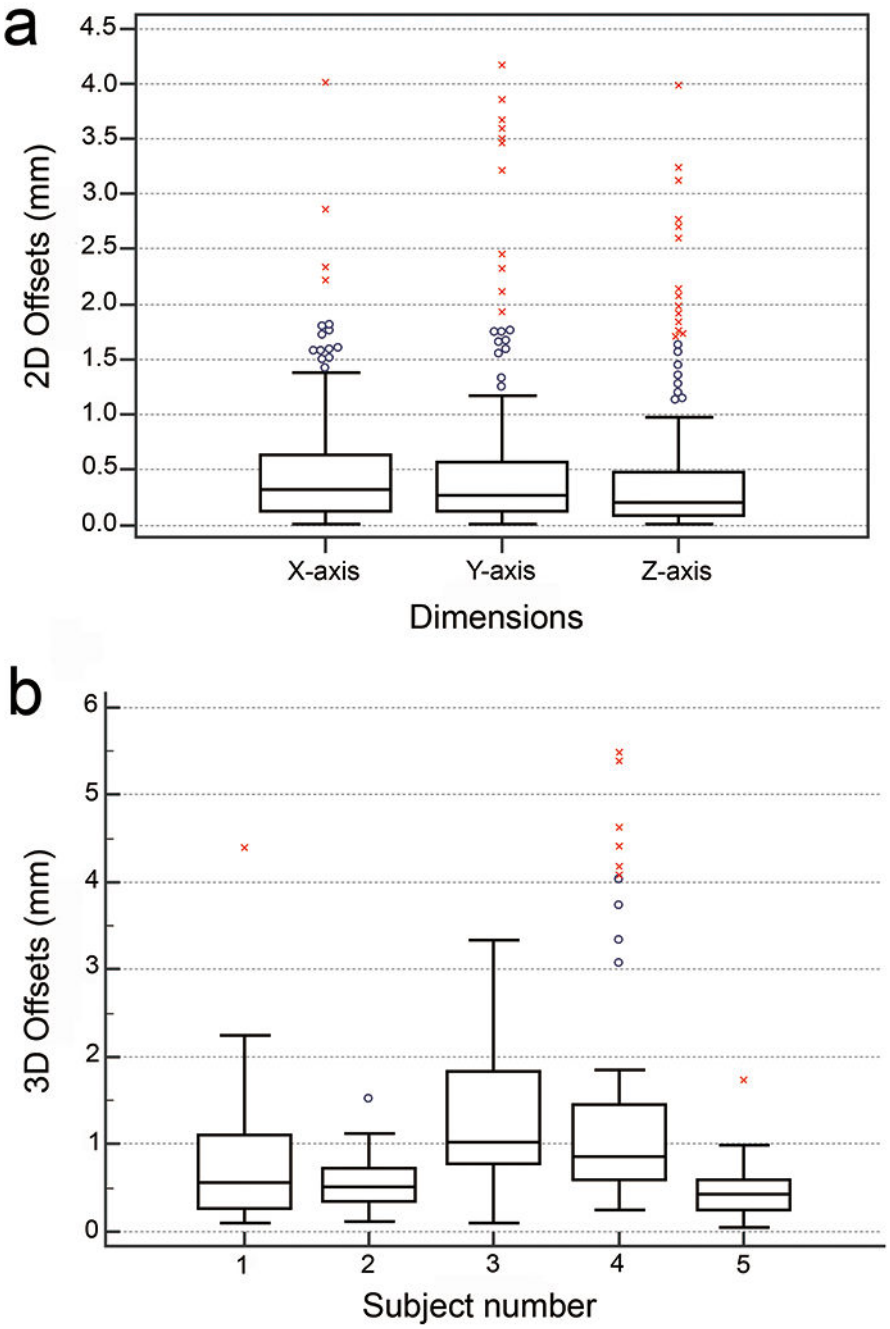

Fig 8.

Box-and whisker plots comparing the offsets in original FE-MRA and fused image within subjects (a) and between subjects (b). The upper and lower line in the box represent the 25th and 75th quartile. The middle line represents the median. The whiskers represent the minimum and maximum values.

Table 1.

The characteristics for all patients included in our study. The patients with pacemaker (subject No. 1-4) and femoral catheter (subject No. 5) were included in a subset analysis for the evaluation of image fusion accuracy.

Subject	Sex	Age (years)	eGFR (mL/min/ 1.7)	MRI scanner	MRI slice thickness (mm)	CT region	CT slice thickness (mm)	IMD
1	F	66	21	Avanto	1.3	1, 2, 3	1	1
2	F	78	27	Avanto	1.3	1	1	1
3	M	69	78	Avanto	1.4	1	1.5	1
4	F	89	35	Avanto	1.3	1	1	1
5	F	46	>89	Trio TIM	1.3	2, 3	2	2
6	F	66	18	Avanto	1.3	1	1	-
7	M	89	53	Prisma	1.2	2, 3	0.75	-
8	F	76	28	Prisma	1.2	1	1.5	-
9	M	80	39	Prisma	1.25	1	1.5	-
10	M	72	54	Trio TIM	1.2	2, 3	1	-
11	F	86	27	Trio TIM	1.2	1, 2, 3	2	-
12	M	71	37	Skyra	1.3	2, 3	2	-
13	M	89	38	Prisma	1.4	1	3	-
14	M	79	20	Prisma	1.2	2	2	-
15	F	83	36	Prisma	1.3	1, 2, 3	1.5	-

*CT regions: 1=chest, 2=abdomen, 3=pelvis

**Implantable medical device (IMD): 1=pacemaker, 2=catheter

eGFR, estimated glomerular filtration rate; F, female; M, male